World Academy of Science, Engineering and Technology
International Journal of Electronics and Communication Engineering
Vol:4, No:9, 2010

Modeling and Visualizing Seismic Wave Propagation in Elastic Medium Using Multi-Dimension Wave Digital Filtering Approach

Jason Chien-Hsun Tseng, Nguyen Dong-Thai Dao, and Chong-Ching Chang

***Abstract*—**A novel PDE solver using the multidimensional wave digital filtering (MDWDF) technique to achieve the solution of a 2D seismic wave system is presented. In essence, the continuous physical system served by a linear Kirchhoff circuit is transformed to an equivalent discrete dynamic system implemented by a MD wave digital filtering (MDWDF) circuit. This amounts to numerically approximating the differential equations used to describe elements of a MD passive electronic circuit by a grid-based difference equations implemented by the so-called state quantities within the passive MDWDF circuit. So the digital model can track the wave field on a dense 3D grid of points. Details about how to transform the continuous system into a desired discrete passive system are addressed. In addition, initial and boundary conditions are properly embedded into the MDWDF circuit in terms of state quantities. Graphic results have clearly demonstrated some physical effects of seismic wave (P-wave and S–wave) propagation including radiation, reflection, and refraction from and across the hard boundaries. Comparison between the MDWDF technique and the finite difference time domain (FDTD) approach is also made in terms of the computational efficiency.

***Keywords*—**Seismic Wave Propagation, Multi-dimension Wave Digital Filters, Partial Differential Equations.

I. Introduction

THE modeling of multi-dimension (MD) physical system is of great importance to engineering and science for describing many phenomena that occur in nature including acoustic seismic exploration, acoustic electromagnetic, fluid flow, etc. The most popular kind of model for MD physical systems are partial differential equations (PDEs) with properly imposed initial and boundary conditions. In most cases of practical interest, the differential equations cannot be solved analytically and so numerical approaches are sought. Techniques such as finite differences, finite elements and waveguides [1] have been used in some success and various algorithms have been developed to implement these techniques.

Jason Chien-Hsun Tseng is with the Department of Information Engineering Kun Shan University, Taiwan (corresponding author to provide e-mail: jt571029@mail.ksu.edu.tw)

Nguyen Dong-Thai Dao is with the Graduate Institute of Mechatronic System Engineering, National University of Tainan, Taiwan (e-mail: thaipr.action@gmail.com)

Chong-Ching Chang is with the Graduate Institute of Mechatronic System Engineering, National University of Tainan, Taiwan (e-mail: jeff0718@mail.nutn.edu.tw)

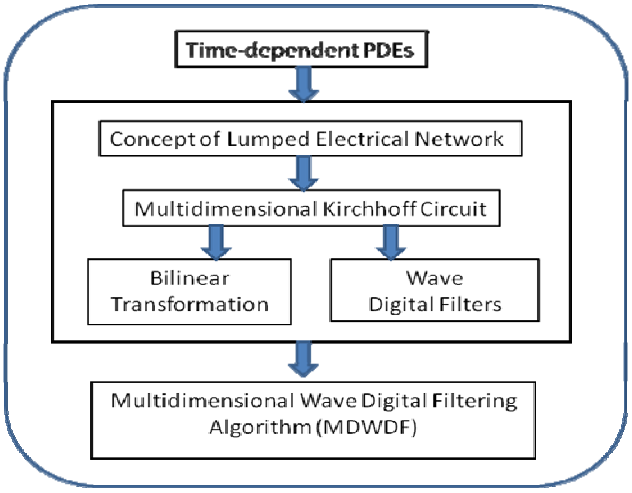

Fig. 1 A general schematic diagram of the MDWDF circuit modeling procedure

While there are always debates regarding performance, each method offers its own advantages and drawbacks. In this contribution, we make use of the MDWDF technique [2], an alternative approach to the PDE system integration, for modeling the behavior of physical wave propagation in 2D elastic media, particularly in the field of seismic wave propagation in rock seam. The attraction of the MDWDF approach is that it possesses a variety of outstanding features that make this concept better off than those conventional numerical approaches mentioned above. The main distinct of a MDWDF model includes:

- High accuracy due to the use of the WDF structure as is known to have low round off noise characteristics [3].
- MD passivity, which guarantees the robustness and basically all numerical stability properties [4].
- Full local interconnectivity due to the generation of a 2^{nd} order difference equation relating the value of a point on the grid to its previous values of nearest-neighborhood grid points [2]. Other 2^{nd} order methods do not offer this property.

In the context of seismology application, numerical modeling of seismic wave propagation in the elastic media has become of increasingly economic importance in recent year due to geological complexity of regions and difficulties in conducting the seismic surveys in the area. An important

application is the seismic reflection survey, which is the most widely used geophysical exploration approach in the petroleum industry. Two different body waves propagation are concerned for in-seam seismic study: P-wave (primary wave or compressional wave), and S-wave (secondary wave or shear wave) [5-6]. The aim of our study is to present a full derivation of a suitable MDWDF algorithm for numerical modeling and visualization of these body waves propagation within an elastic medium (e.g. the medium of rock).

The technique starts with details of a 2D acoustic seismic system modeling. It then follows by a network description of the system for which inductors are introduced to validate passivity of the electronic circuit followed by the Kirchhoff rules. From this mechanism, a lumped multidimensional Kirchhoff circuit (MDKC) is developed whose behaviors are entirely equivalent to the system of PDEs itself. Applying the bilinear transformation or a generalized trapezoidal rule [2] to all reactive elements of the MDKC together with the standard wave digital principles, a discrete-time equivalence called MDWDF circuit is obtained to numerically implement the continuous physical system. This way the differential equations used to describe elements of a MD passive electronic circuit is approximated by a grid-based difference equations implemented by the so-called state quantities within the passive MDWDF circuit. So the model can track the wave field on a dense 3D grid of points. A general schematic diagram showing the MDWDF circuit modeling procedure is illustrated in Fig. 1. As the MDWDF circuit contains no information on the initial and boundary conditions, accommodation of initial and boundary conditions to the MDWDF circuit body in terms of state quantities are also discussed. Numerical simulation to visualize some physical behaviors of these seismic waves propagation within a specified geometry field is studied.

II. Problem Definition

Let us consider the propagation of a 2D scalar acoustic seismic wave in rock seam where the system can be mathematically described as the following channel wave [5, 6]:

$$c^2\nabla^2 p = \frac{\partial^2 p}{\partial t^2} + f \tag{1}$$

Here $p=p(x,z,t)$ denotes the pressure of seismic wave propagating in the underground concrete rock seam, c is the speed of sound in the medium and $f=f(x,z,t)$ is an external body force per unit volume. Although spanned in the pair of 2D rectangular coordinates (x, z) in Eq. (1), the 2nd order hyperbolic PDE system contains representatives' seismic fluid speeds in every direction of axes. Assume the density of the medium ρ_0 is homogeneous throughout the medium and define the vector form of the acoustic velocity $\mathbf{v}(\mathbf{x},t)=[v_x(\mathbf{x},t),v_z(\mathbf{x},t)]^T$

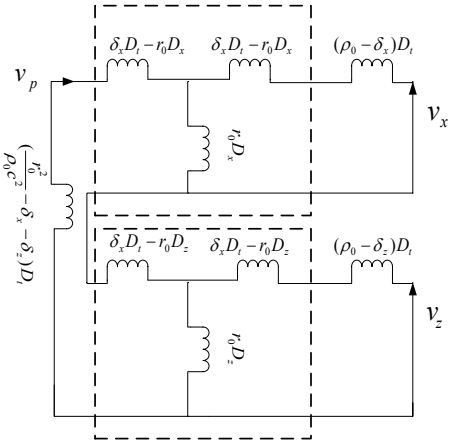

Fig. 2 MD Kirchhoff circuit representation of the 2D seismic system.

where $\mathbf{x}$ is a vector of space coordinates x, z and t denotes time. The wave field in the2nd order system (1) can then be recast into a coupled 1st order systems of PDEs governing the equations of motion and continuity [5-7]:

$$\left.\begin{aligned} \rho_0 \frac{\partial}{\partial t}\mathbf{v}(\mathbf{x},t) + \nabla\, p(\mathbf{x},t) = 0 \\ \frac{1}{\rho_0 c^2}\frac{\partial}{\partial t}\, p(\mathbf{x},t) + \nabla\cdot\mathbf{v}(\mathbf{x},t) = 0 \end{aligned}\right\} \tag{2}$$

We note that by neglecting the effects of gravity, which is used to form the external body force in Eq. (1), the homogenous system in Eqs. (2) is taken place for finding a suitable MDWDF model in a simplified environment.

III. MD Kirchhoff Network and MDWDF Model

A. MD Kirchhoff Network Realization

Let the operators $D_t(\cdot)$, $D_x(\cdot)$, $D_z(\cdot)$ be denoted by the partial derivatives with respect to the temporal t and spatial coordinates x, z. In order to apply the circuit theory for representing the behavior of the system, the same physical dimension must be kept for all field variables. As a result, the velocity amplitude v_p is introduced in terms of the complex pressure amplitude p with an arbitrary real impedance r_0, i.e. $v_p = p/r_0$. Note that r_0 plays an important role in the development of MDWDF model to determine properties of the resulting algorithm and is limited only by the stability considerations. Based on the definition of v_p , the PDE system (2) can be written as a set of symmetric hyperbolic PDEs:

$$\left.\begin{aligned} \rho_0 D_t(v_x(\mathbf{x},t)) + r_0 D_x(v_p(\mathbf{x},t)) = 0 \\ \rho_0 D_t(v_z(\mathbf{x},t)) + r_0 D_z(v_p(\mathbf{x},t)) = 0 \\ r_0 D_x(v_x(\mathbf{x},t)) + r_0 D_z(v_z(\mathbf{x},t)) \\ + \frac{r_0}{\rho_0 c^2} D_t(v_p(\mathbf{x},t)) = 0 \end{aligned}\right\} \tag{3}$$

Using principles of the circuit theory, the system (3) can be immediately realized as mesh equation of a 3D Kirchhoff circuit depicted in Fig. 2 with mesh currents v_x, v_z, v_p. We note that techniques of the circuit theory applied to represent the pressure-velocity PDEs of Eq. (3) in terms of network inductors cannot be realized by real world components. Instead, the network is a graphical representation of time and space differentiation operation. Consequently, a flux notation in Fig. 2, such as $(\rho_0 - \delta_x)D_t(v_x)$, may be interpreted as a mesh voltage across an inductor with inductance $L = (\rho_0 - \delta_x) \geq 0$ pushing the time-varying mesh current v_x to flow through the inductor. In addition, passivity of the inductances involving the derivative operator D_t is realized with carefully selected auxiliary constants, i.e. $0 < \delta_x, \delta_z \leq \rho_0$ and $\delta_x + \delta_z \leq r_0^2 / \rho_0 c^2$. The symmetric 2-port T-circuit in the MDKC representation of Fig. 1 can be replaced by its corresponding Jaumann structure [3], a well-known grounded lossless two-port equivalent of the symmetric lattice, which is comprised of two inductors and an ideal transformer with transformation ratio -1/1. This important property guarantees an explicit algorithm after some forms of discrete realization using the WDF-based properties [3].

B. MDWDF Circuit Arrangement

To arrive at an approximation of each mesh voltage across the corresponding inductance in the MDKC of Fig. 2, a generalized trapezoidal rule [2] is applied to the integration of each mesh voltage. The resultant coordinates $[x,t]^T=[mT_x,nT_z,kT_t]^T$, $(m,n,k \in N)$ takes only discrete values with the temporal step size T_t, and the spatial step sizes T_x and T_z in x and z coordinates, respectively. Furthermore, port resistances r_1, r_2 for the two-port Jaumann filters and resistances r_j', $j=1, 2, 3$ for the self-inductors are obtained, respectively, given by

$$\left.\begin{aligned} r_1' = \frac{2(\rho_0 - \delta_x)}{T_t}, r_2' = \frac{2(\rho_0 - \delta_z)}{T_t} \\ r_3' = 2\left(\frac{r_0^2}{\rho_0 c^2} - \delta_z - \delta_x\right)/T_t \end{aligned}\right\} \quad (4)$$

When the passivity is held for mesh inductance in the MDKC, a lower bound of a ratio between the density of sampling in time and that of sampling in space is obtained, i.e.

$$T_0 / T_t \geq \sqrt{2} v_0 \quad (5)$$

Here $T_0 \equiv \sqrt{T_x^2 + T_y^2} / \sqrt{2}$ is defined as the smallest spatial step against the largest temporal step T_t. In addition, $v_0 = \sqrt{\rho_0} c$ represents the irrotational phase velocity of a seismic wave traveling freely across the whole area according to the 2nd order system in system (1). This result is the well known Courant-Friedrichs-Levy (CFL) bound [7], which guarantee numerical stability of the wave equations adopted by many numerical approaches. For a simplified MDWDF circuit, the least restriction on the ratio for given densities of the sampling in space has yielded $T_x = T_z \equiv h$ that implies

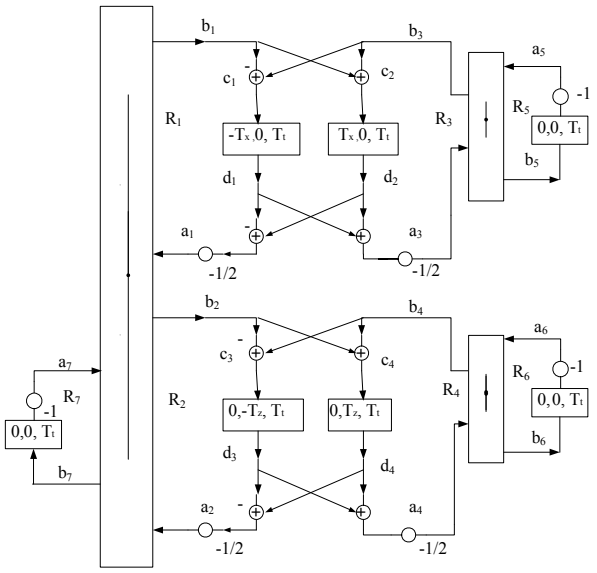

Fig. 3 MDWDF circuit for the discrete modeling of the seismic system.

$$\delta_x = \delta_y = \rho_0, r_0 = \sqrt{2}\rho_0 c \quad (6)$$

Let us adopt the voltage wave principle, which defines the forward wave and backward wave quantities a_v and b_v, respectively, as the pressure wave quantities according to [2]:

$$a_v = p_v + R_v v_v, b_v = p_v - R_v v_v \quad (7)$$

Here R_v is the port resistance, a positive constant. Combining with the generalized trapezoidal rule, which processes the continuous system of a Jaumann two-port branch to its equivalent WDF structure [2], we may transform the reference MDKC to its corresponding WDF structure. This yields the MDWDF circuit illustrated in Fig. 3 for numerically modeling behaviors of the pressure-velocity PDE system (1). In view of the MDWDF circuit, its structure contains two 2-port series adaptors on the right hand side and one 3-port series adaptor on the left hand side. These port adaptors are then coupled by two Jaumann wave digital filters with shift operations in space and time. Define the mesh current for various series ports according to the WDF principles:

$$v_x = v_3 = v_5 = \frac{a_3 - b_3}{2R_3} = \frac{a_5 - b_5}{2R_5} \quad (8)$$

$$v_z = v_4 = v_6 = \frac{a_6 - b_6}{2R_6} = \frac{a_4 - b_4}{2R_4} \quad (9)$$

$$v_p = v_1 = v_2 = v_7 = \frac{a_1 - b_1}{2R_1} = \frac{a_2 - b_2}{2R_2} = \frac{a_7 - b_7}{2R_7} \quad (10)$$

The signal flow for each port adaptor within the MDWDF circuit can be described by

$$\left.\begin{aligned} b_3 &= a_3 - \bar{r_3}(a_3 + a_5); \bar{r_3} = \frac{2R_3}{R_3 + R_5} \\ b_5 &= a_5 - \bar{r_5}(a_3 + a_5); \bar{r_5} = \frac{2R_5}{R_3 + R_5} \end{aligned}\right\} \tag{11}$$

$$\left.\begin{aligned} b_4 &= a_4 - \bar{r_4}(a_4 + a_6); \bar{r_4} = \frac{2R_4}{R_4 + R_6} \\ b_6 &= a_6 - \bar{r_6}(a_4 + a_6); \bar{r_6} = \frac{2R_6}{R_4 + R_6} \end{aligned}\right\} \tag{12}$$

$$\left.\begin{aligned} b_1 &= a_1 - \bar{r_1}(a_1 + a_2 + a_7); \bar{r_1} = \frac{2R_1}{R_1 + R_2 + R_7} \\ b_2 &= a_2 - \bar{r_2}(a_1 + a_2 + a_7); \bar{r_2} = \frac{2R_2}{R_1 + R_2 + R_7} \\ b_7 &= a_7 - \bar{r_7}(a_1 + a_2 + a_7); \bar{r_7} = \frac{2R_7}{R_1 + R_2 + R_7} \end{aligned}\right\} \tag{13}$$

The port resistances R_i, $i=1,...,7$, due to the generalized trapezoidal rule, can also be chosen as follow:

$$\left.\begin{aligned} R_1 = R_3 = r_1, r_1 &\equiv \frac{r_0}{T_x} = \frac{\delta_x}{T_t} \\ R_2 = R_4 = r_2, r_2 &\equiv \frac{r_0}{T_z} = \frac{\delta_z}{T_t} \\ R_5 = r'_1, R_6 = r'_2, R_7 &= r'_3 \end{aligned}\right\} \tag{14}$$

Referring back to the MDWDF circuit, the relations of waves and states quantities can be realized as

$$\left.\begin{aligned} &d_1 + d_2 + 2a_3 = 0 \\ &d_3 + d_4 + 2a_4 = 0 \\ &d_2 - d_1 + d_4 - d_3 + 2(a_1 + a_2) = 0 \end{aligned}\right\} \tag{15}$$

$$\left.\begin{aligned} &b_2 + b_4 = c_4 \\ &b_1 + b_3 = c_2 \\ &b_3 - b_1 + b_4 - b_2 = c_1 + c_3 \end{aligned}\right\} \tag{16}$$

Furthermore, the state input-output relations within the lattice wave digital filters are described as

$$\left.\begin{aligned} d_1(mT_x, nT_z, kT_t) &= -c_1((m+1)T_x, nT_z, (k-1)T_t) \\ d_2(mT_x, nT_z, kT_t) &= -c_2((m-1)T_x, nT_z, (k-1)T_t) \\ d_3(mT_x, nT_z, kT_t) &= -c_3(mT_x, (n+1)T_z, (k-1)T_t) \\ d_4(mT_x, nT_z, kT_t) &= -c_4(mT_x, (n-1)T_z, (k-1)T_t) \end{aligned}\right\} \tag{17}$$

Following from Eqs. (5)-(16), the desired wave variables can now be expressed in the form of state output d_j as

$$v_x(\mathbf{x},t) = \frac{-\bar{r}_3}{2R_3}\left[\frac{d_1(\mathbf{x},t) + d_2(\mathbf{x},t)}{2} + a_5(t)\right] \tag{18}$$

$$v_z(\mathbf{x},t) = \frac{-\bar{r}_6}{2R_6}\left[\frac{d_3(\mathbf{x},t) + d_4(\mathbf{x},t)}{2} + a_6(t)\right] \tag{19}$$

$$p(\mathbf{x},t) = \frac{-r_0\bar{r}_1}{2R_1}\left[\frac{d_2(\mathbf{x},t) - d_1(\mathbf{x},t) + d_4(\mathbf{x},t) - d_3(\mathbf{x},t)}{2} + a_7(t)\right] \tag{20}$$

The model (and thus the system variables stated in Eqs. (18)-(20)) can now be simplified by assuming that the lossless conditions in Eq. (3.4) hold for the CFL limit. It can be verified that the aforementioned assumptions lead to

$$\left.\begin{aligned} &R_7 = R_5 = R_6 = 0; R_1 = R_2 = R_3 = R_4 = R_0 \\ &b_3 = -a_3; b_4 = -a_4; b_1 = -a_2; b_2 = -a_1 \\ &a_5 = a_6 = a_7 = 0 \end{aligned}\right\} \tag{21}$$

Redefining the time step size $T_t=T$, we thus simplified the MDWDF circuit notations as

$$R_0 = \frac{2\rho_0}{h} = \frac{2r_0}{T}, h = \sqrt{2}Tc \tag{22}$$

Accordingly, the field variables expressed in Eqs. (18)-(20) is recast as

$$v_x(\mathrm{x},t) = \frac{-1}{2R_0}[d_1(\mathrm{x},t) + d_2(\mathrm{x},t)] \tag{23}$$

$$v_z(\mathrm{x},t) = \frac{-1}{2R_0}[d_3(\mathrm{x},t) + d_4(\mathrm{x},t)] \tag{24}$$

$$p(\mathrm{x},t) = \frac{-r_0}{2R_0}[d_2(\mathrm{x},t) - d_1(\mathrm{x},t) + d_4(\mathrm{x},t) - d_3(\mathrm{x},t)] \tag{25}$$

IV. Treatment of Initial and Boundary Conditions

Because the system (2) (and hence the resultant MDWDF algorithm of Fig. 3) describes only the free-space propagation, it has to be accomplished by initial and boundary conditions when finite energy and finite enclosures are present. In this section, imposed conditions described by state equations will be properly embedded into the MDWDF circuit.

A. Initial Conditions

Let the general initial conditions (ICs) of the system (2) be imposed as follows:

$$\left.\begin{aligned} p(\mathrm{x},0) &= \alpha_p(\mathrm{x}) \\ \left.\frac{\partial p(\mathrm{x},t)}{\partial t}\right|_{t=0} &= \beta_p(\mathrm{x}) \end{aligned}\right\} \tag{26}$$

$$\left.\begin{aligned} v(\mathrm{x},0) &= \alpha_v(\mathrm{x}) \\ \left.\frac{\partial v(\mathrm{x},t)}{\partial t}\right|_{t=0} &= \beta_v(\mathrm{x}) \end{aligned}\right\} \tag{27}$$

where $\alpha_v \equiv [\alpha_x, \alpha_z]^T$ and $\beta_v \equiv [\beta_x, \beta_z]^T$ are defined as a vector form. We first consider the first set of ICs in Eq. (26) with zero order derivative by focusing on the pressure amplitude $p(\mathbf{x},t) = r_0 v_p(\mathbf{x},t)$ *at* $t=0$. Substituting the initial value in Eq. (26) into Eq. (20) simply yields (indices $(\mathbf{x},0)$ and $(\mathbf{x})$ are omitted)

$$\frac{r_0\bar{r}_1}{2R_1}[\frac{-[d_2-d_1+d_4-d_3]}{2}+a_7(0)]-\alpha_p=0 \tag{28}$$

In view of Eq. (28), the wave quantity a_7 remains unknown as involving only in the time shift of the MDWDF circuit. Thus, one needs to concern with the 1st order derivative of Eqs. (26). By considering the mesh voltage p_7 across the time-dependent self-inductor with the inductance $L = r^2_0/\rho_0 c_2-\delta_x-\delta_z$ in the MDKC, i.e. $p_7(x,t)=L_7\partial v_7(x,t)/\partial t$, we obtain

$$a_7(0)=\frac{R_7}{r_0}[\alpha_p+\frac{T_t}{2}\beta_p] \tag{29}$$

as a result of taking time derivative of the pressure amplitude, and substituting v_7 and initial value into Eqs. (11) and (26). Making use of Eqs. (9)-(14), the 2nd set of ICs can also be stated in terms of the state equations (indices (**x**,0) and (**x**) are omitted):

$$\left.\begin{aligned}&\frac{\bar{r}_3}{2R_3}[\frac{-[d_1+d_2]}{2}+a_5(0)]=\alpha_x\\&a_5(0)=\frac{R_5}{r_0}[\alpha_x+\frac{T_t}{2}\beta_x]\end{aligned}\right\} \tag{30}$$

$$\left.\begin{aligned}&\frac{\bar{r}_6}{2R_6}[\frac{-[d_3+d_4]}{2}+a_6(0)]=\alpha_z\\&a_6(0)=\frac{R_6}{r_0}[\alpha_z+\frac{T_t}{2}\beta_z]\end{aligned}\right\} \tag{31}$$

Now we substitute the forward wave quantities in Eqs. (28)-(31) into Eqs. (15), and define $d_1=f(x)$ to yield their corresponding state output representation as follows:

$$\left.\begin{aligned}d_1&=f(x)\\d_2&=-2a_3-f(x)\\d_4&=-a_4+\frac{R_1}{r_0\bar{r}_1}\alpha_p(x)-a_7+a_3+f(x)\\d_3&=-\frac{R_1}{r_0\bar{r}_1}\alpha_p(x)+a_7-a_3-f(x)\end{aligned}\right\} \tag{32}$$

B. Boundary Conditions

Let us consider a closed finite enclosure of the system (1) whose piecewise smooth boundary surface can be simply stated by the reflection property. Accordingly, the system variable such as the pressure p on the boundary can be read by $p=Zv$ with the boundary surface impedance Z perpendicular to its corresponding velocity v with the implementation of perfectly match layers (PMLs). Originally developed by Berenger [8], the technique specifies a new region that surrounds the MDWDF domain where a set of non physical equations are applied giving a high attenuation. To shorter our discussion, we consider the simplified MDWDF circuit with a rectangular system of dimension $l_x\times l_z$ as depicted in Fig. 4. The wave source is marked with S and travelling inside the

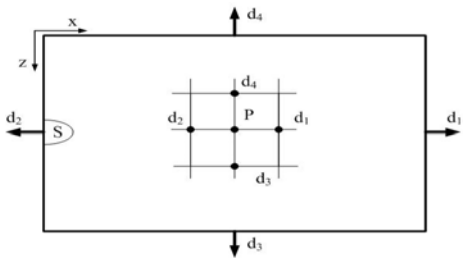

Fig. 4 Part of grid points within the medium *M* for the rectangular seismic system.

medium *M* with surface impedance Z_x and Z_z set along with the *x*- and *z*-direction, respectively. For any inner point P on the spatial sampling grid and at a certain sampling time $t=kT$, its grid value according to Eq. (17) is determined by four state output points:

$$\left.\begin{aligned}d_1(x,z,t)&=-c_1(x+h,z,t)\\d_2(x,z,t)&=-c_2(x+h,z,t)\\d_3(x,z,t)&=-c_3(x,z+h,t)\\d_4(x,z,t)&=-c_4(x,z-h,t)\end{aligned}\right\} \tag{33}$$

While still true for these four outputs to influence any P on the straight line edges and the rectangular vertices, there is one (or two) of the neighborhood point(s) may be outside the boundary. For the vertices, two adjacent points are outside the boundary by a spatial step size *h*, i.e. (d_1,d_4), (d_4,d_2) and (d_2,d_3) *or* (d_3,d_1). Our aim is to find the expression of these undetermined state outputs that accommodate the boundary condition $p=Zv$ without involving the state inputs, which are generally not computable. Since the reflection property can provide only one solution, one shall need an additional condition, which is imposed by either Eq. (23) or (24) with zero velocity. For instance, when the unknown vertices are (d_1,d_4), the state output d_1 can be obtained by substituting $p=Z_z v_x$ into Eqs. (23) and (25) to yield

$$d_1=\frac{d_2(r_0-Z_z)+r_0(d_4-d_3)}{r_0+Z_z} \tag{34}$$

Referring back to Eq. (24) with $v_z=0$ assumed at the vertex, it simply yields $d_4=-d_3$. The set of vertices (d_1,d_4), thus, are determined. We note that the surface impedance Z_z is related to the reflection coefficient r_f, which is defined by

$$r_f\equiv\frac{Z_z-R_0}{Z_z+R_0}\text{ and }0\le r_f\le 1 \tag{35}$$

Similarly, one can also obtain the sampling grid value for the pressure variable *p* at other vertices, boundaries and inner points at the time point $t=kT$.

V. Numerical Results

In this section, the MDWDF circuit developed previously is present for numerical simulation of the acoustic seismic system inside the elastic medium of rock seam. More specifically, we demonstrate the physical behaviors of the P-wave (longitudinal wave) and S-wave (transverse wave) propagation including radiation, reflection, and refraction from and across the hard boundary. Application of a seismic reflection is also carried out to investigate the locus of all possible underground scatter points. In addition, comparison between the MDWDF technique and the finite difference time domain (FDTD) approach is made in terms of the computational efficiency. Initial value of the static density of rock is set at ρ_0=2200 kg/m³, as well as c_p=2000m/s and c_s=1400m/s denoting as the speed of P–wave and S-wave [6], respectively. The rectangular simulation plane as depicted in Fig. 5(a) is limited by the size of $lx \times lz = 1500 \times 2000$ *m* with the acoustic source located at (-1000,-750). The reflection coefficients for boundaries are set at r_f=0.999 (highly reflective) and r_f =0.001 (highly absorptive) for the sideline surface along the *z*- and *x*-direction, respectively. Figs. 5(a)-(d) shows four subsequent snapshots of synthetic seismic body waves with dominant P-wave propagation from and across the boundaries with various physical effects commonly known in seismology. Fig. 6 explores the difference between the P-wave and S-wave within a synthetic body wave at a specific time slot. Due to its physical behaviors, the longitudinal (P) wave depicted in Fig. 6(a) shows faster propagation as compared with the transverse (S) wave depicted in Fig. 6(b). This is because the S-wave does not change the volume of the material through, which it propagates. Furthermore, as indicated inside the red frame, Fig. 6(a) shows P waves that has particle motion in the direction of travel towards the east boundary. In contrast, Fig. 6(b) shows S waves propagation that has particle motion perpendicular to the direction of travel. To fully explore the behaviors of seismic wave, a seismic reflection survey is also carried out to investigate the locus of all possible underground scatter points, which are assumed to be centered at (500,-750) with the radius of 100m and r_f=0.999 as illustrated in Fig. 7(a). With two intense acoustic sources planted at the locations of (0,0) and (1000,0), and propagated downward of the medium, four subsequent snapshots of Figs. 7(a)-(d) are present to demonstrate acoustic waves reflected back to the surface when these waves reach an interface between rock layers where the density changes in terms of reflection coefficient. Based on the MDWDF domain with the fixed spatial step, the computational efficiency between the FDTD and MDWDF is made, which can be viewed in Fig. 8 and listed in Table 1 for detail. Clearly, the MDWDF is more computationally efficient than the FDTD as the seismic wave simulated by the MDWDF takes less time to travel between boundaries.

VI. Conclusion

In this contribution, the MD wave digital filter structure (MDWDF circuit), an alternative approach to the PDE system integration, was derived from first principles to perform the physical system modeling for the seismic wave propagation in 2D elastic media. In particular, initial and boundary conditions were properly embedded into such a model in a very simple and efficient manner without the modification of the whole circuit body. Simulation results obtained for physical behaviors of the body wave propagation including P-wave and S-wave propagation, and seismic reflection survey have demonstrated the capacities of the MDWDF approach in correctly and effectively modeling the 2D seismic system. Computational efficiency of the MDWDF technique was also confirmed as compared to the FDTD method. The 2D system, we have investigated, provided sufficient and fundamental structure, which enables us to further explore the seismic wave propagation in 3D elastic media. This is the subject of ongoing research

Acknowledgment

This work is supported by NSC (Taiwan) under grant no.: NSC 98-2221-E-168-028.

References

[1] O. Julius Smith III's, A Basic Introduction to Digital Waveguide Synthesis, CCRMA, Stanford University, 2006.

[2] A. Fettweis and G. Nitsche, "Numerical integration of partial differential equations using principles of multidimensional wave digital filters", J. of VLSI Sig. Proc., vol. 3, pp. 7-24, 1991.

[3] A. Fettweis, "Wave digital filter: theory and practice", Proc. IEEE, vol. 74, no. 2, pp. 270-327, 1986.

[4] A. Fettweis, ``Robust numerical integration using wave-digital concepts," Multidim. Syst. Sig. Process, Vol. 17, pp. 7-25, 2006.

[5] A. Udias, Principles of seismology, Cambridge University Press, 1999.

[6] L. Dresen "The influence of an asymmetry in the sequence rock-coalrock on the propagation of Rayleigh seam waves", Geophysical Prospecting, 1985.

[7] P. K. Kundu, Fluid Mechanics, Academic Press Limited, London, 1990.

[8] J. P. Berenger, "A perfectly matched layer for the absorption of electromagnetic waves'. J. Computational Physics, vol 114, 185-200, 1994.

TABLE 1 COMPUTATIONAL EFFICIENCY BETWEEN THE FDTD AND MDWDF

Range (m)	FDTD (ms)	MDWDF (ms)
166	4.084	4.521
500	15.578	15.776
707	38.644	32.682
1666	60	58.8
1760	94	82.9
3330	114.04	101.143

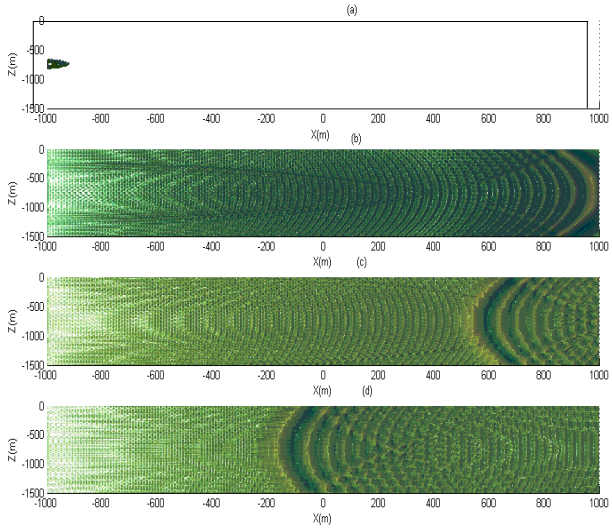

Fig. 5 Propagation of synthetic seismic body wave with dominant P-wave at four time slots: (a) t =0. (b) t = 1025 ms. (c) t = 1237 ms . (d) t = 1590 ms.

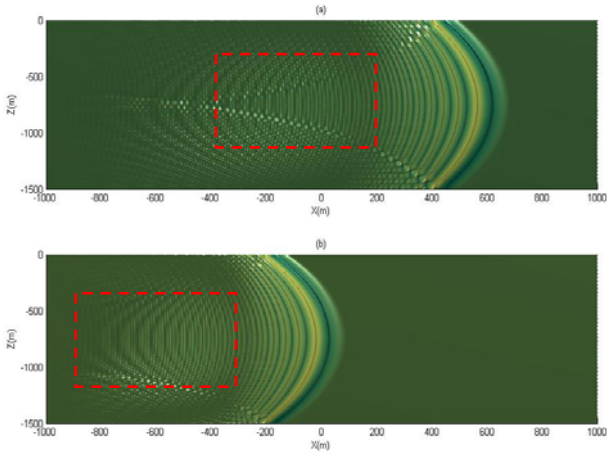

Fig. 6 The difference between P- and S-waves propagation at t=813 ms within a synthetic body wave: (a) P-wave propagation indicated within the red frame has particle motion in the direction of travel towards the east boundary. (b) S-wave propagation within the red frame has particle motion perpendicular to the direction of travel.

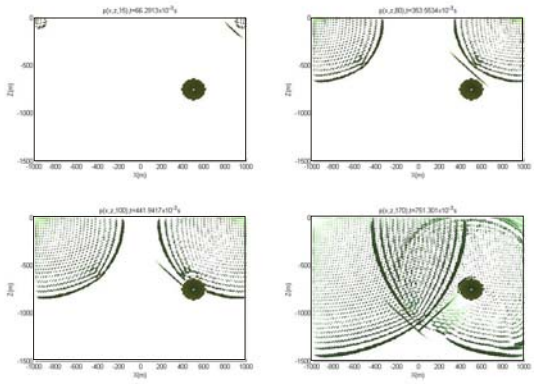

Fig. 7 Four subsequent snapshots of reflection seismic waves to investigate the locus of all possible underground scatter points centered at (500,-750) with the radius of 100m and r_f=0.999.

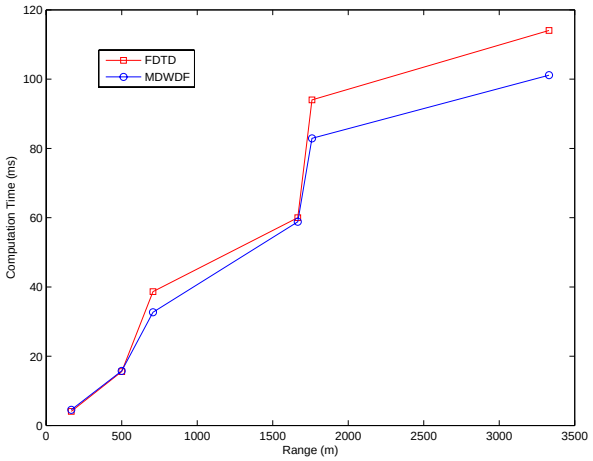

Fig. 8 The computational efficiency between the FDTD marked by red-square and MDWDF marked by blue-circle.